Journal of Rock Mechanics and Geotechnical Engineering 10 (2018) 703–716

Contents lists available at ScienceDirect

Journal of Rock Mechanics and Geotechnical Engineering

journal homepage: www.rockgeotech.org

Full Length Article

Physical modeling of behaviors of cast-in-place concrete piled raft compared to free-standing pile group in sand

Mehdi Sharafkhah, Issa Shooshpasha*

Faculty of Civil Engineering, Babol Noshiravani University of Technology, Shariati Av., Babol, Mazandaran, Iran

ARTICLE INFO

Article history:
Received 16 September 2017
Received in revised form
4 December 2017
Accepted 28 December 2017
Available online 30 April 2018

Keywords:
Free-standing pile group
Piled raft
Pile–soil–raft interaction
Physical modeling
Cast-in-place concrete piles

ABSTRACT

Similar to free-standing pile groups, piled raft foundations are conventionally designed in which the piles carry the total load of structure and the raft bearing capacity is not taken into account. Numerous studies indicated that this method is too conservative. Only when the pile cap is elevated from the ground level, the raft bearing contribution can be neglected. In a piled raft foundation, pile–soil–raft interaction is complicated. Although several numerical studies have been carried out to analyze the behaviors of piled raft foundations, very few experimental studies are reported in the literature. The available laboratory studies mainly focused on steel piles. The present study aims to compare the behaviors of piled raft foundations with free-standing pile groups in sand, using laboratory physical models. Cast-in-place concrete piles and concrete raft are used for the tests. The tests are conducted on single pile, single pile in pile group, unpiled raft, free-standing pile group and piled raft foundation. We examine the effects of the number of piles, the pile installation method and the interaction between different components of foundation. The results indicate that the ultimate bearing capacity of the piled raft foundation is considerably higher than that of the free-standing pile group with the same number of piles. With installation of the single pile in the group, the pile bearing capacity and stiffness increase. Installation of the piles beneath the raft decreases the bearing capacity of the raft. When the raft bearing capacity is not included in the design process, the allowable bearing capacity of the piled raft is underestimated by more than 200%. This deviation intensifies with increasing spacing of the piles.

1. Introduction

The conventional approach for the design of piled raft foundations basically ignores the raft load-sharing, and it has been assumed that the piles carry the whole of structural loads. This approach is unduly conservative and leads to an uneconomic design. Only when the pile cap is elevated from the ground level (i.e. free-standing pile group), this design method is valid. Poulos and Davis (1980) suggested that for sandy soil, the bearing capacity of a piled raft could be considered as the sum of the ultimate bearing capacities of the raft plus all the piles. This approach is called “new approach” in this paper.

A piled raft foundation consists of three main components: piles, soil and raft (Reul and Randolph, 2004). Although there are a vast analytical and numerical researches about these foundations (Dung et al., 2010; Raut et al., 2014; Comodromos et al., 2016; Alnuaim et al., 2017; Huang et al., 2017), the experimental studies are limited. The available laboratory studies mainly concern the behavior of the piled raft by physical modeling.

Lee and Chung (2005) found if piles were installed in a small space, the stresses and strains of the surrounding soil would be overlapped, and the bearing behavior of the piles would be different from that of the single pile. They also found that during pile driving, the soil density increased when the pile spacing to diameter ratio (s/d) was less than three.

Fioravante and Giretti (2010) indicated that at the initial steps of loading due to higher stiffness of piles than surrounding soil, the loads were transmitted to the piles mostly. Thus at these steps, the slope of the load-settlement curve in the piled raft is steeper compared to unpiled raft. As the soil failed at the shaft and the point of the piles, the stiffness of the piled raft was approximately equal to that of unpiled raft with an identical slope of the load-settlement curve. Poulos and Davis (1980) also found a similar result and presented a simplified curve for the piled raft.

* Corresponding author.
E-mail address: shooshpasha@nit.ac.ir (I. Shooshpasha).
Peer review under responsibility of Institute of Rock and Soil Mechanics, Chinese Academy of Sciences.

https://doi.org/10.1016/j.jrmge.2017.12.007

El Sawwaf (2010) defined a bearing pressure improvement (BPI) ratio, which is the ratio of the bearing pressure of a piled raft to that of an unpiled raft at the same settlement level. El-Garhy et al. (2013) carried out 40 small-scale tests on single pile, unpiled raft and piled raft with central piles in sand. They also studied the effects of the raft thickness and rigidity on the results. Bazyar et al. (2009) carried out a 1g physical modeling test and concluded that the physical modeling of the piled raft could be the best way of calibrating design calculation.

Without considering scale effect in an experimental model, the application of obtained results is limited to the same model. Sedran et al. (2001) related that with a ratio of footing diameter to grain size greater than 30, the influence of grain size on model response could be neglected. Tagaya et al. (1988) also reported the similar results. According to Altaee and Fellenius (1994), the soil used in 1g physical modeling must be loose sufficiently.

In the abovementioned laboratory researches, metal piles (aluminum or steel) were used, and the pile models were installed by driving or jacking into the soil. The angles of friction between pile and soil in cast-in-place bored concrete piles are different from that of steel piles. Unlike cast-in-place bored concrete pile, in driven piles, soil density increases during driving.

The current study concentrates on physical modeling of piled rafts under vertical axial load in the laboratory in which cast-in-place bored concrete piles and reinforced concrete raft are used. The test models in this research include single pile, single pile in pile group, unpiled raft, free-standing pile group with 4 or 9 piles, and piled rafts with 4 or 9 piles. Some instruments record the load contribution between the piles and the raft. The effect of the pile installation in the group is also investigated. By comparing the measured bearing capacities of free-standing pile group and piled raft with the same number of piles, the differences between the traditional and new approaches in the piled raft design are studied. The effects of the number and spacing of piles on the settlement and bearing capacity of the foundation are also evaluated.

2. Test models, material and setup

2.1. Test models

In this study, cast-in-place bored concrete piles are used. The dimensions of the piles after extracting from the soil are measured. The diameter and embedded length of the piles are 2.84 cm and

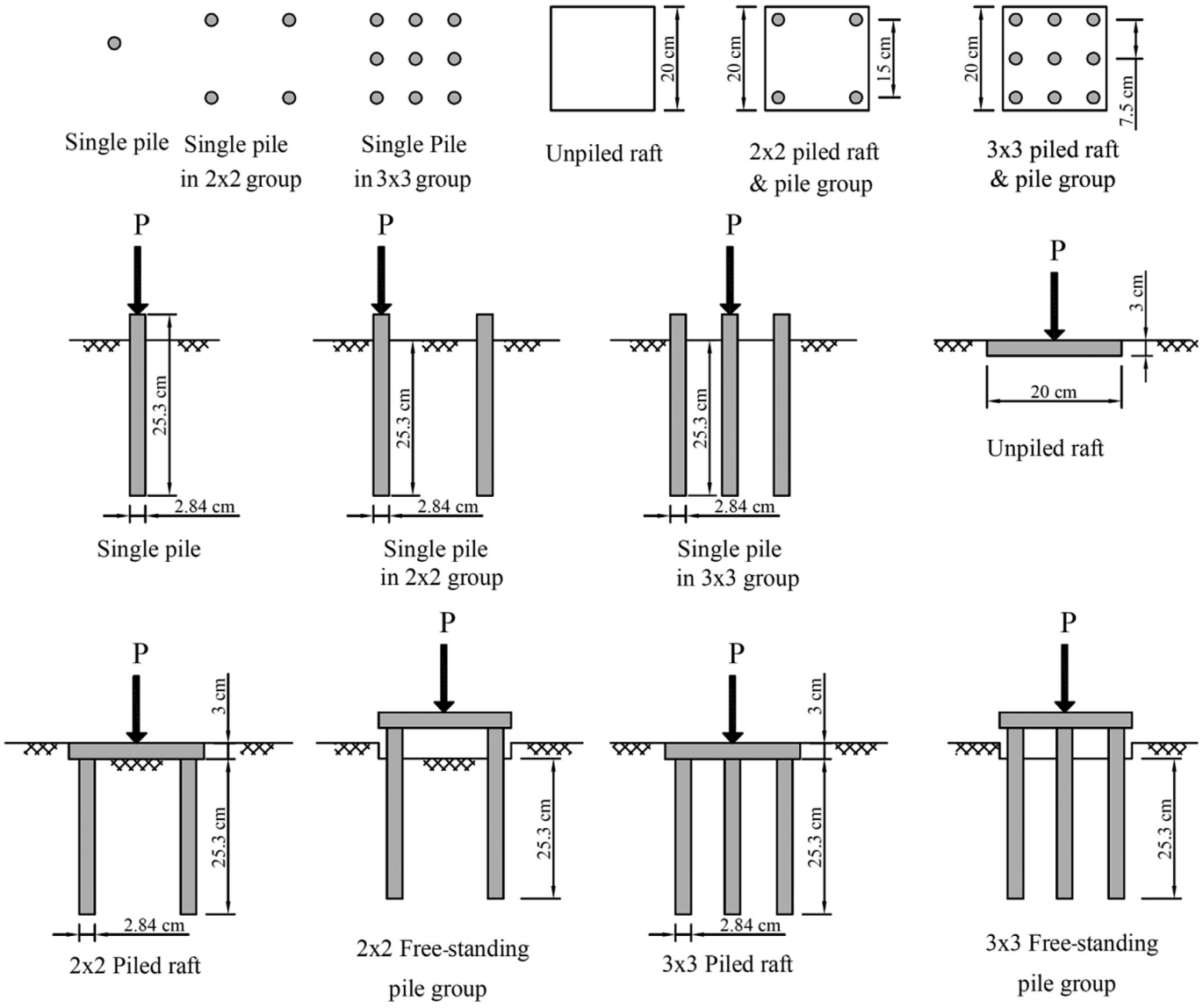

Fig. 1. Schematic of test models.

25.3 cm, respectively. Therefore, the length to diameter ratio is 8.91. It is assumed that the piles are rigid, thus the settlements at the top and bottom of the piles are assumed identical. The raft model is square shaped (20 cm × 20 cm) and its thickness is 3 cm. The raft is made of cast-in-place reinforced concrete. The types of the test models used are shown in Fig. 1. The pile spacing to diameter ratios (s/d) for the models with 4 and 9 piles are 5.2 and 2.6, respectively. Test models and their labels are as follows: unpiled raft R (#), single pile S (#), single pile in pile group SG (#), free-standing pile group with 4 and 9 piles FG-4 (#) and FG-9 (#), and piled rafts with 4 and 9 piles PR-4 (#) and PR-9 (#). Each test repeats once and the symbol # represents the sequence of tests.

2.2. Test material

Dry Babolsar sand is used for the test. The minimum and maximum unit weights of the soil are 14.9 kN/m^3 and 17.6 kN/m^3, respectively, and the specific gravity is measured to be 2.79. The soil gradation curve is shown in Fig. 2. The effective grain size (D_{10}), uniformity coefficient (C_u) and curvature coefficient (C_c) are measured to be 0.11, 2.6 and 1.09, respectively. The sand is classified as SP according to the unified soil classification system. The mean grain size is 0.26 mm and thus the ratio of the pile diameter to mean grain size is calculated as approximately 109. Therefore, the grain size effect could be ignored. According to Altaee and Fellenius (1994), the test soil should be loose sufficiently. With this condition, the responses of the test model and the prototype are similar. Therefore, in this research, the sand with relative density of 30% is used. The peak and constant-volume angles of internal friction of the sand are 37° and 34°, respectively, from triaxial tests. The compressive strengths of the concrete raft and piles are 25 MPa and 10 MPa, respectively, and their unit weights are 22.6 kN/m^3 and 20.8 kN/m^3, respectively.

2.3. Test setup

In order to conduct the tests, a square box is prepared. The box sidewalls are made of steel frames to increase its rigidity. Inner dimensions of this box are 1.3 m × 1.3 m and its height is 1 m. This box is located on a rigid reinforced concrete slab with dimensions of 2.2 m × 2.2 m and 30 cm in height. The distance between the center of the test model to the edge of the box is three times greater than the raft width, and the distance between the pile tips to the bottom of the box is two times greater than the pile length. With these considerations, the end effects of the box side could be ignored. Four transparent Plexiglas plates are covered around the box for observation of soil surface level during filling. A steel frame provides the support needed for loading. The frame consists of two steel rods connecting a sufficiently rigid beam to the base concrete. Beneath the beam, a hydraulic jack is placed. The test load is applied by a transfer rod to the load cell and then to the model. In order to hold the hydraulic jack over the model and beneath the beam constant, two steel plates are used. The first plate is placed on the top of the beam and the second beneath the hydraulic jack, which is connected to the top plate. In the bottom plate, in order to provide the free movement of the shaft during loading, a hole with a diameter of 100 mm is designed. Since one of the research purposes is to measure the differential settlement and the tilt, five dial gages are used for the tests. One dial gage in the center, two in the corner and two in the middle side of the raft are placed. For single pile, two dial gages in the opposite side of the pile are installed on the two reference beams, which are located on the box edge sides. These instruments are shown in Fig. 3.

3. Testing procedure

For achieving a homogenous soil, the sand is poured into the box in layers with thickness of 10 cm and relative density of 30%. The height of the soil at the end of the filling is 80 cm. A wooden plate with dimensions of 20 cm × 20 cm connected to a wooden rod is used to compact the soil layers. For construction of the piled raft, a thin wall square tube with inner dimensions of 20 cm × 20 cm and depth of 5 cm and wall thickness of 1 mm is lowered into the soil, and subsequently, the inside of the box is excavated. A wooden template is placed into the box and the pile casings are located into the template and the upper part of the soil. The wooden template is used to determine the accurate place of the piles and provide guidance for them. The external diameter, length and thickness of the pile casings are 25 mm, 350 mm and 1.2 mm, respectively. The casing is lowered down manually by about 5 cm and the inside soil is drilled simultaneously with a hand auger. This operation is

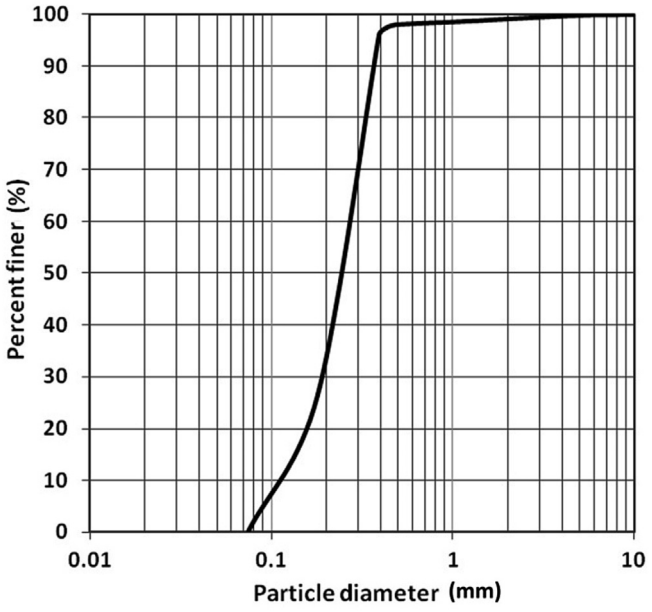

Fig. 2. Grain size distribution of the test sand.

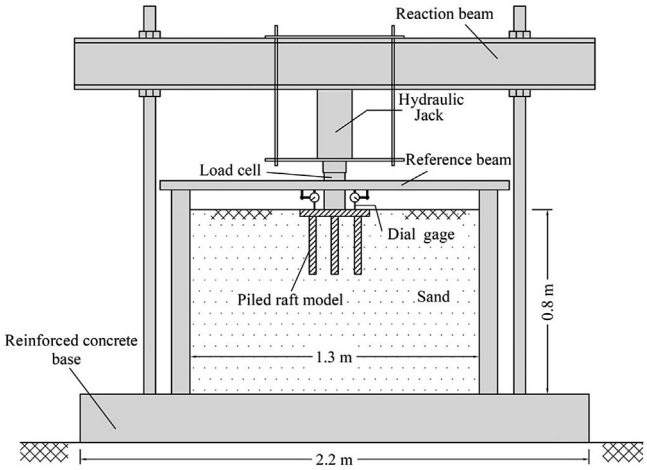

Fig. 3. Schematic of test setup.

continued step by step until the embedment length of the casing reaches 25 cm. In order to construct test models, all casings are placed into the soil. The inside height of the casings should be approximately equal to the pile length. Then casting the concrete is initiated. The casings are extracted during pouring concrete. This action as well as placement of casing should be done slowly and carefully. Finally, the template must be extracted.

In order to measure the stress and load distribution, a number of load and pressure cells are placed on the piles and beneath the raft, respectively. Configuration of pressure cells changes according to model type and pile arrangement, and the cells are usually installed at the corner, middle of edge, center of the raft, and the adjacent area of the piles. Fig. 4 shows the names and configuration of these instruments for the unpiled raft and piled raft models.

In the piled raft models, the level of the pile head is equal to that of surrounding soils on which the raft was built. In order to construct the single pile or free-standing pile group, the pile head is elevated about 5 cm by a guide mold. Therefore, it is assured that the load is not transferred to the soil. At the next stage, a 3 × 3 rebar mesh is located at the bottom of the raft base, and the concrete is cast.

A steel plate of 9 cm in diameter and 5 cm in thickness is placed in the center of the raft on the fresh concrete. It is used for decreasing stress concentration. At the end, the square box is extracted from the edge of the raft slowly. During construction of the free-standing pile group, the pile head is elevated about 5 cm from the surrounding soil, and the load cells are installed on the planned piles. In these cases, polystyrene foam is placed on the piles initially and the cap is constructed above it. The polystyrene foam is removed after the concrete reaches necessary strength. The dimensions of each test model are measured after loading test and discharging of the soil.

In order to measure the vertical settlement of the foundations, five dial gages are installed over the cap with precision of 0.01 mm and travel of 50 mm. The constant load is applied incrementally. In piled raft and unpiled raft, each load increment is maintained for 3 min until the rate of settlement is not greater than 0.03 mm/min. For single pile and free-standing pile group, when the rate of settlement reduces to 0.25 mm in an hour, the test is stopped. The total applied load is measured by a load cell. During the test on the single pile, the loading is continued until the settlement equals 15% of the pile diameter. The piled raft and free-standing pile group tests are ended when the maximum settlement reaches 15% of the cap width or failure occurs. Each test is repeated once to control result accuracy.

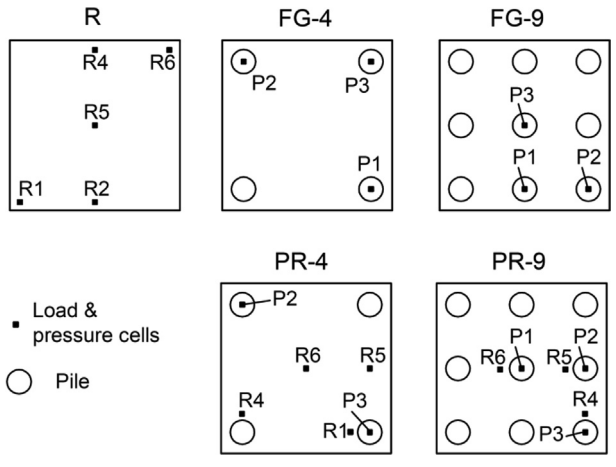

Fig. 4. Schematic of instrument names and configuration for the unpiled raft and piled raft models.

4. Results and discussion

4.1. Loading test results for single pile

The pile dimensions after extracting from the soil are measured. The pile diameter and embedded length are 2.84 cm and 25.3 cm, respectively. The increase of pile diameter from 25 mm to 28.4 mm is due to the penetration of fresh concrete into the adjacent soil. The result of the loading test on a single pile is shown in Fig. 5. The ultimate bearing capacity of the pile is estimated to be 0.44 kN, which is determined as the load indicated by the intersection of tangent lines drawn through the initial, flatter portion of the total settlement curve and the steeper portion of the same curve (Tomlinson, 2004). In order to evaluate the effect of pile installation on other piles, the loading test is carried out on the single pile in a group. Fig. 6 demonstrates the results of these tests in 2 × 2 and 3 × 3 groups.

In Fig. 7, the load-settlement curve of the single pile is compared with the single pile in the group. By installation of a single pile in a group, the pile bearing capacity and stiffness increase. The bearing capacities of the central, middle side and corner piles in the 3 × 3 group are increased by 57%, 36% and 11%, respectively. This value is about 5% for corner piles located in the 2 × 2 group. Corner piles have lower stiffness and bearing capacity than others. The piles located in the 2 × 2 group show a similar behavior as the corner piles in the 3 × 3 group. The stiffness and bearing capacity of the central pile are increased due to pile confinement generated by adjacent piles and increase of soil density caused by casing penetration. In fact, the confinement increases equivalent stiffness of the soil-pile composition around the pile that decreases soil deformation and pile settlement. Furthermore, due to arching effect, the stress around the pile increases and as a result, the pile ultimate bearing capacity increases.

4.2. Loading test results for free-standing pile group

The results of loading test on the 2 × 2 and 3 × 3 free-standing pile groups are shown in Fig. 8 for two successive tests, and their averages are demonstrated in Fig. 9. The load-settlement relations of the piles in the free-standing group are shown in Figs. 10 and 11. Figs. 12 and 13 show the comparisons of the average load-settlement relations of single pile in a group with the pile in free-standing group.

The behaviors of the piles in the 2 × 2 free-standing pile groups are approximately similar, but those in the 3 × 3 free-standing pile groups depend on their positions. Similar to single pile in pile group, the bearing capacity of the central pile is the greatest, followed by edge pile and corner pile. The bearing capacity of the pile

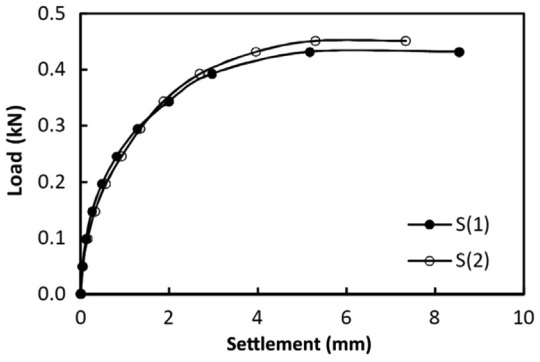

Fig. 5. Load-settlement relations of single piles.

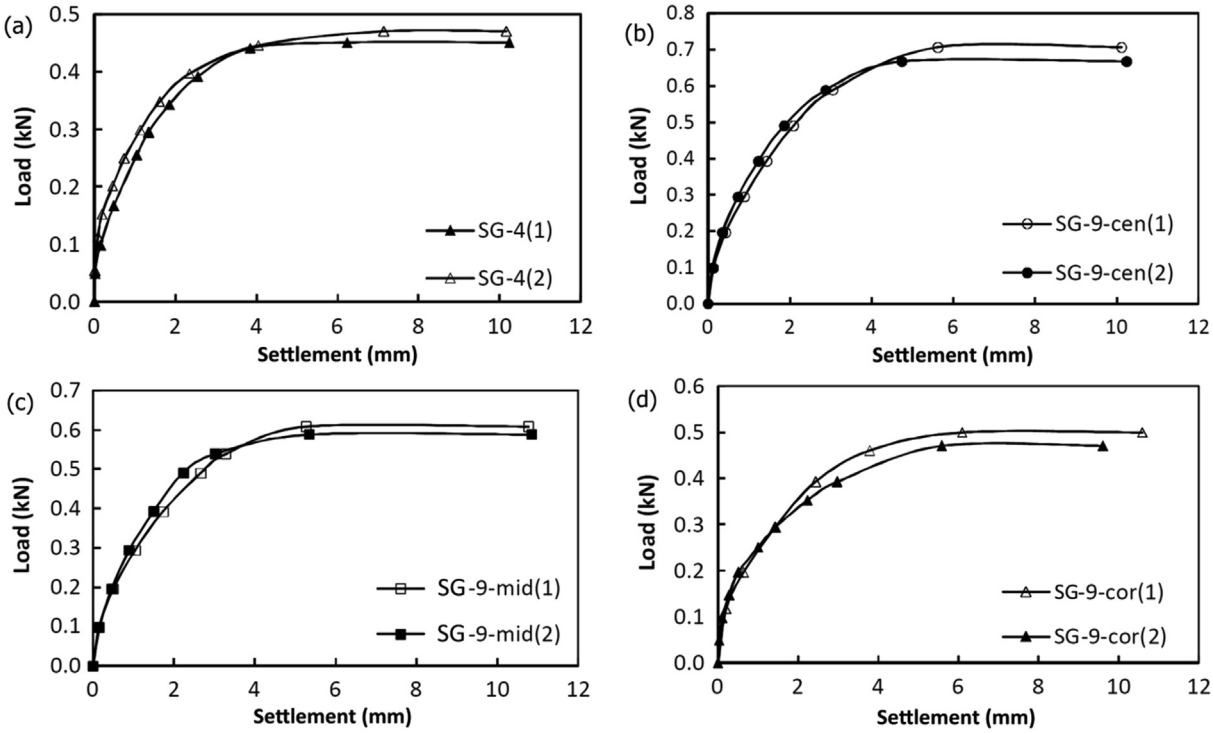

Fig. 6. Load-settlement relations of single piles in a group for two successive tests: (a) 2 × 2 pile group; (b) central pile in 3 × 3 pile group; (c) middle side pile in 3 × 3 pile group; and (d) corner pile in 3 × 3 pile group.

in free-standing group is approximately equal to that of corresponding single pile in group, but the pile stiffness in the free-standing group is less due to the pile stress interaction during loading. On the other hand, the pile settlement in free-standing group increases in comparison to single pile in the corresponding group under the same load. In addition, for the same reason, the pile bearing capacity in the 3 × 3 pile group is slightly greater than that for the corresponding single pile. In the 2 × 2 free-standing group, due to larger spacing between the piles ($s/d = 5.2$), the stiffness reduction is less than that in the 3 × 3 group ($s/d = 2.6$).

4.3. Loading test results for piled raft

In order to compare free-standing groups with piled rafts, a series of loading tests is conducted on unpiled raft, 2 × 2 and 3 × 3 piled rafts, and each test is repeated once. Figs. 14 and 15 show the comparisons of load-settlement curves of piles located beneath the raft, in which Δ_{max} is the maximum settlement. The corner pile

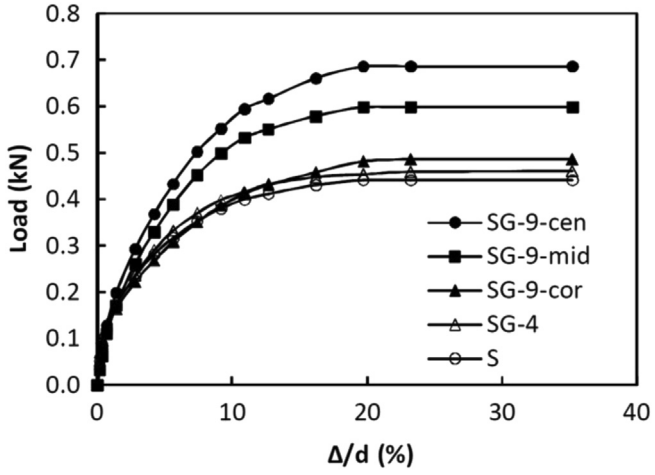

Fig. 7. Average load-settlement relations of single pile and single pile in group. Δ is the settlement and d is the pile diameter.

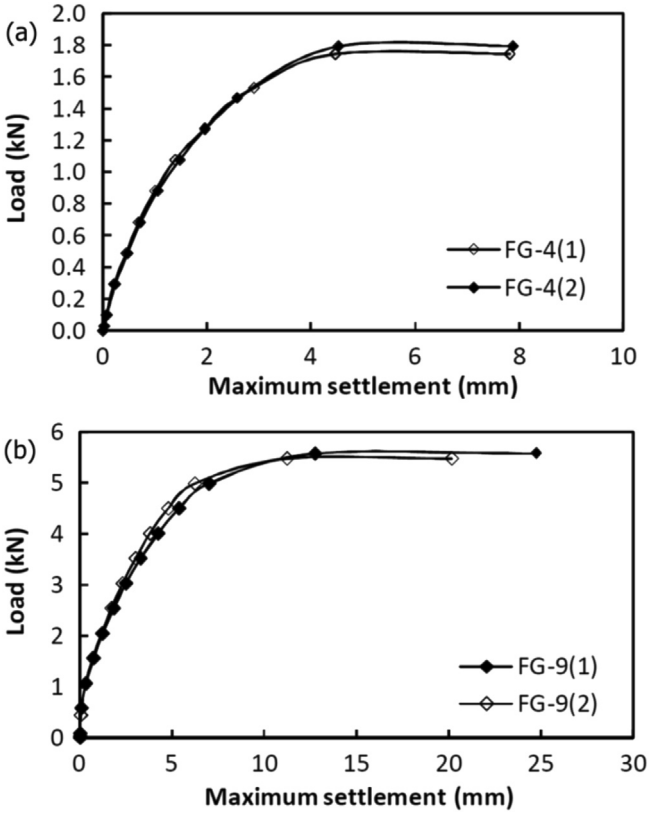

Fig. 8. Load-settlement relations for free-standing pile groups: (a) 2 × 2 and (b) 3 × 3 free-standing pile groups for two successive tests.

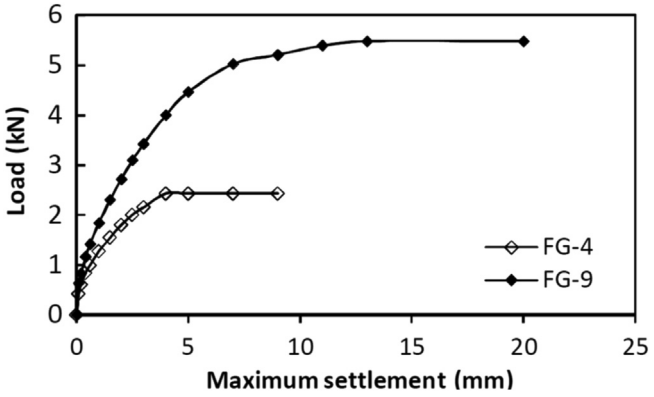

Fig. 9. Average load-settlement relations for 2 × 2 and 3 × 3 free-standing pile groups.

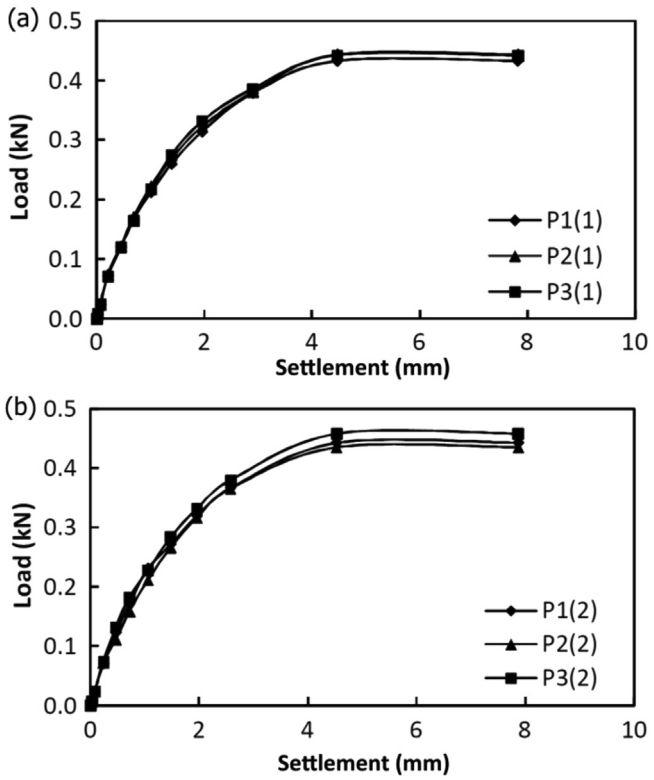

Fig. 10. Load-settlement relations of corner piles in 2 × 2 free-standing pile group for two successive tests.

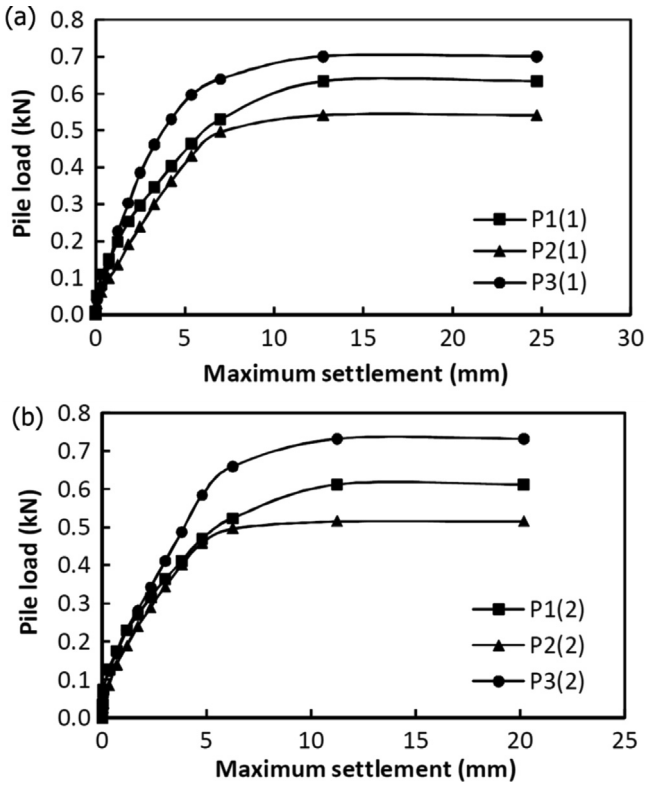

Fig. 11. Load-settlement relations of middle side, corner and central piles in 3 × 3 free-standing pile group for two successive tests.

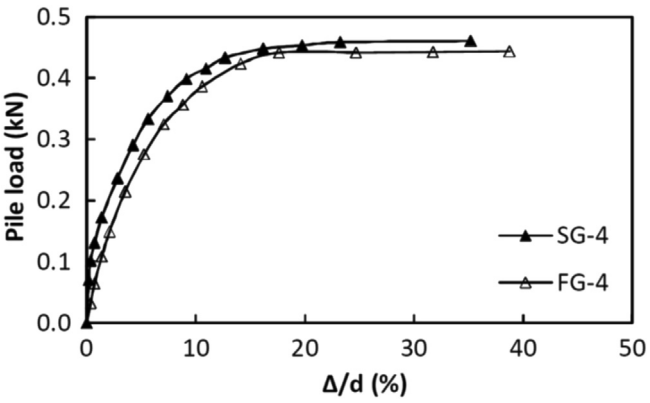

Fig. 12. Average load-settlement relations of single piles in 2 × 2 group and 2 × 2 free-standing pile group.

curves coincide with each other in the 2 × 2 and 3 × 3 piled rafts. At the beginning of the loading, the stiffnesses of corner piles are greater than those of other piles. Fig. 15 presents a comparison of the load-settlement curves for a single pile in the corner of pile group, the corner piles in the 2 × 2 piled raft and 2 × 2 free-standing pile group. In the piled raft, after pile failure, due to the increase in the stress around the piles caused by the raft pressure, a hardening phenomenon occurs. In the central piles and the middle side piles, due to negative friction caused by the raft pressure, the pile bearing capacity increases gradually. In the corner piles, because of the lower raft pressure, the hardening phenomenon is insignificant.

Fig. 16 shows the comparison of load-settlement curves of piles in piled raft foundation and free-standing group. The behaviors of the corner piles are approximately similar. Yielding points in corner piles coincide with each other. The slight difference is due to the raft pressure in piled raft that increases the pile bearing capacity. In the other piles due to greater raft pressure and associated negative friction, the pile stiffness decreases and the bearing capacity increases significantly. In the corner, edge and central piles in the 3 × 3 piled raft, the increases in pile bearing capacity in comparison to single pile are approximately 16%, 64% and 264%, respectively.

The averages of measured results of pressure cells installed beneath the raft are shown in Fig. 17. In unpiled raft, the corner, middle side and center of the raft yield consecutively. In other words, with approaching the center of the raft, the raft bearing capacity increases. In fact, because of the stress confinement in the central area, the failure occurs at higher stress level.

In the 2 × 2 piled raft, since the pressure cell installed adjacent to the piles is close to the middle side pressure cell, their curves

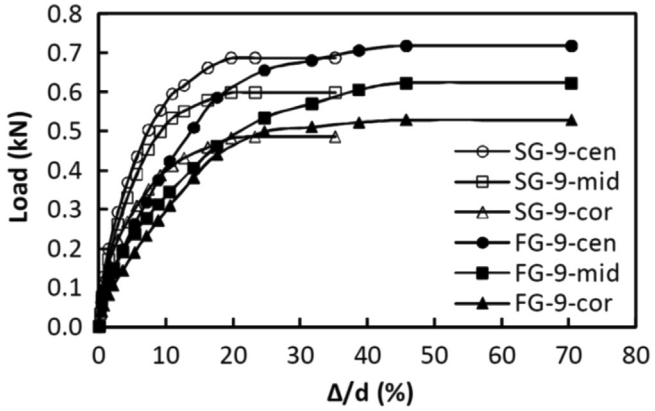

Fig. 13. Average load-settlement relations of single piles in 3 × 3 group and 3 × 3 free-standing group.

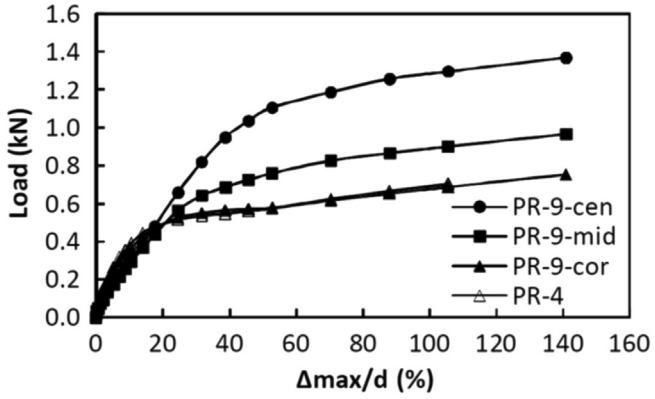

Fig. 14. Average load-settlement relations of piles in 2 × 2 and 3 × 3 piled rafts.

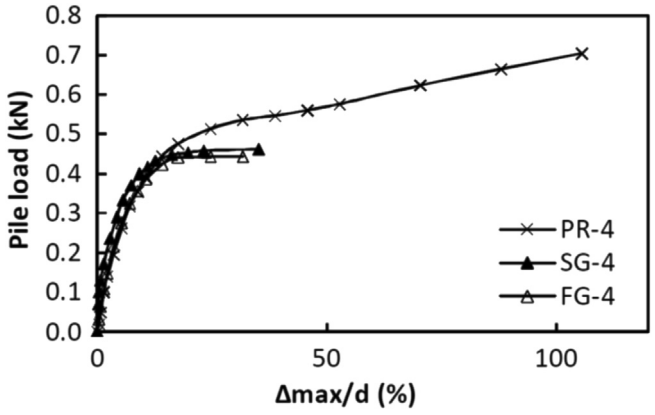

Fig. 15. Average load-settlement relations of piles in 2 × 2 free-standing group and 2 × 2 piled raft and a single pile in group.

become similar. Generally, given that the four corner piles carry a portion of the load symmetrically, the contact pressure beneath the raft is more uniform than other models. In the 3 × 3 piled raft and at the initial steps of loading, the piles carry the most portion of the load. After pile failure, the raft pressure rises suddenly. The pressure increases from the corner to the center of the raft. In the central pile, due to the stress interaction, the pile stiffness is smaller and therefore, the raft pressure in the central area is higher.

Fig. 18 compares the raft pressures in the corresponding points of test models. In the center of the raft, the pressure-settlement

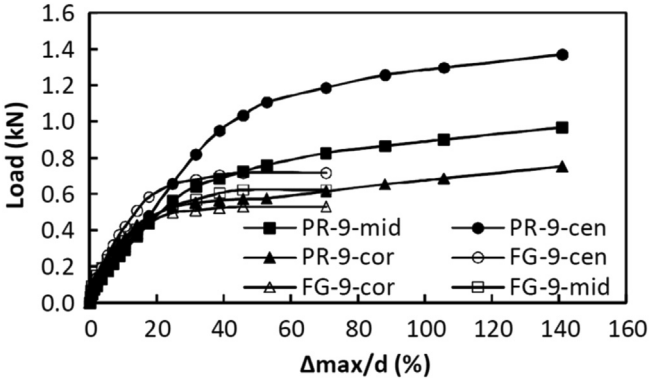

Fig. 16. Average load-settlement relations of piles in 3 × 3 piled raft and 3 × 3 free-standing pile group.

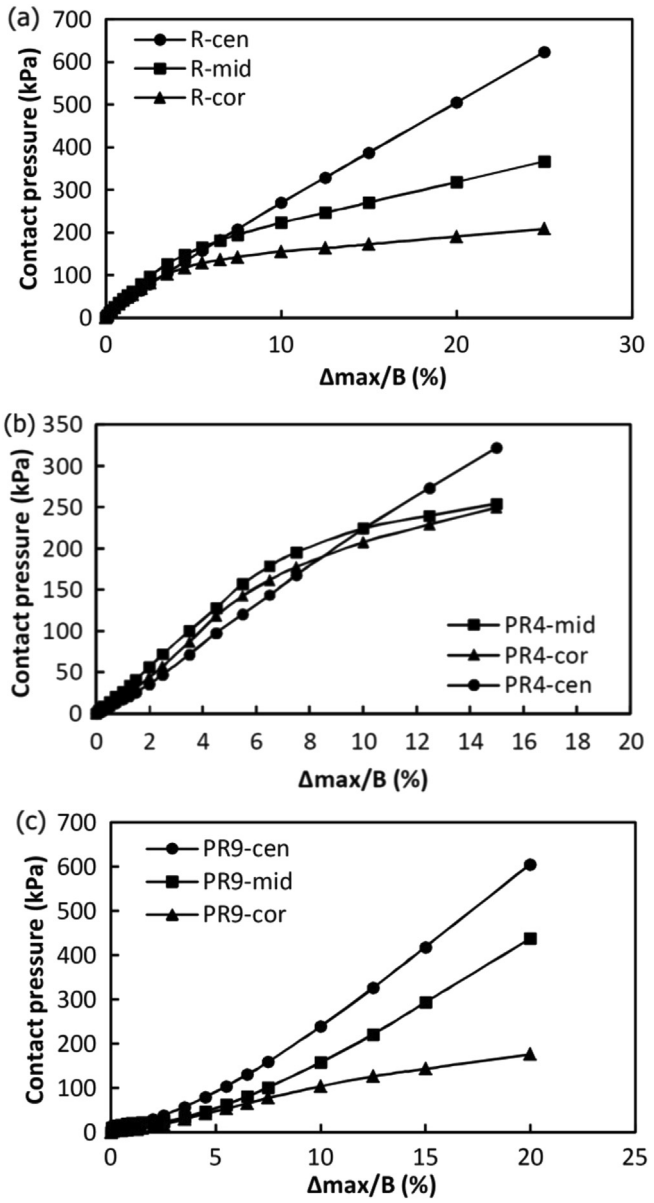

Fig. 17. Average contact pressure-settlement relations beneath the raft: (a) unpiled raft; (b) 2 × 2 piled raft; and (c) 3 × 3 piled raft. *B* represents the raft width.

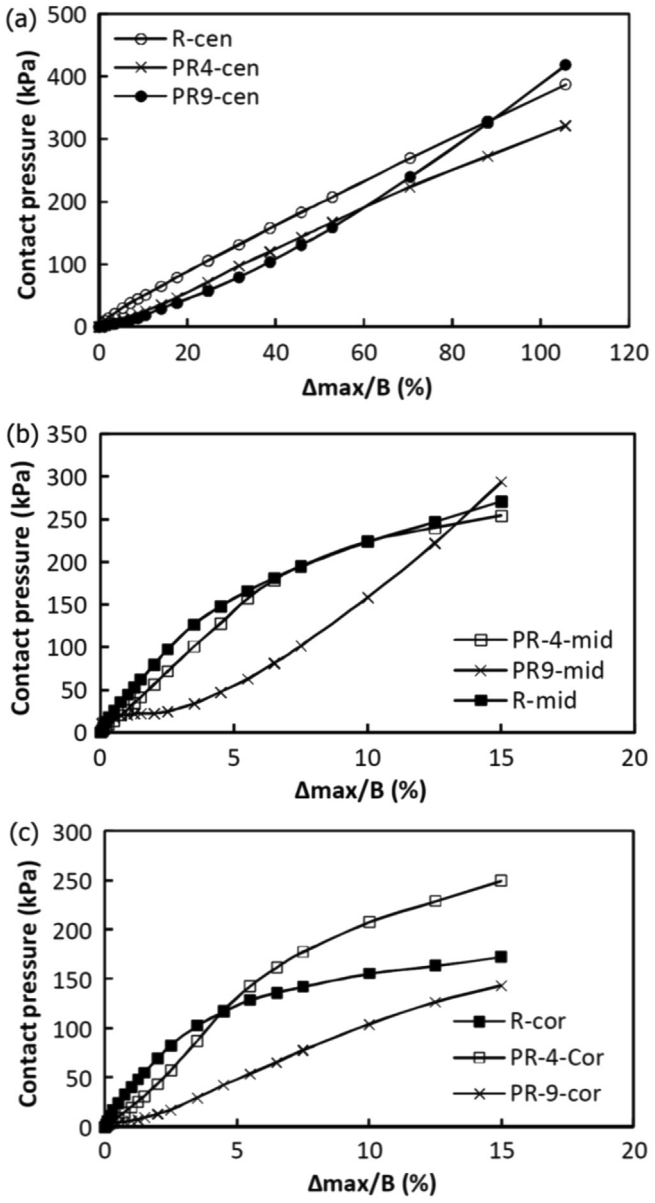

Fig. 18. Average contact pressure-settlement relations for corresponding points: (a) center; (b) middle side; and (c) corner.

curves in the test models show more adjustment. In the corner area, due to greater stiffness of the corner piles, the raft pressure is small initially and then increases after pile failure. Magnitude of the pressure decreases with increasing number of piles.

4.4. Discussion

Table 1 summarizes the measured pile bearing capacities in the models. In this table, P_u and P_a are the ultimate and allowable loads of the piles, respectively; S_{Pu} and S_{Pa} are the corresponding settlements of the piles at the ultimate and allowable loads, respectively. The pile ultimate load is indicated by the intersection of tangent lines drawn through the initial, flatter portion of the total settlement curve and the steeper portion of the same curve (Tomlinson, 2004). The factor of safety in calculating allowable load is considered as 3. For design of the pile group, the effect of pile arrangement on its bearing capacity is usually not considered.

Table 1
Pile load and settlement in the test models.

Model	P_u (kN)	P_a (kN)	S_{Pu}/d (%)	S_{Pa}/d (%)	$P_{a(cal)}$ (kN)	$P_a/P_{a(cal)}$
S	0.44	0.15	19.05	1.14	0.15	1
SG-4	0.46	0.15	19.12	1.08	0.15	1.05
SG-9-cor	0.49	0.16	20.96	1.41	0.15	1.11
SG-9-mid	0.6	0.2	20.01	1.86	0.15	1.36
SG-9-cen	0.69	0.23	20.21	1.88	0.15	1.57
FG-4	0.44	0.15	20.47	2.07	0.15	1
FG-9-cor	0.48	0.16	22.42	4.15	0.15	1.09
FG-9-mid	0.6	0.2	37.75	3.83	0.15	1.36
FG-9-cen	0.72	0.24	47.34	4.71	0.15	1.64
PR-4	0.49	0.16	20.66	2.7	0.15	1.11
PR-9-cor	0.51	0.17	22.64	2.89	0.15	1.16
PR-9-mid	0.72	0.24	45.17	8.17	0.15	1.64
PR-9-cen	1.16	0.39	64.71	13.93	0.15	2.64

In Table 1, $P_{a(cal)}$ is the calculated allowable load used in the usual design calculations, and it is assumed equal to the measured allowable load of single pile. $P_a/P_{a(cal)}$ is the ratio of the measured to calculated allowable loads in each test. This ratio represents the amount of deviation occurred in the design process. The ratio is calculated as 2.64 for central pile in the 3 × 3 piled raft. It means that the measured bearing capacity of the central pile is greater than two times of the corresponding value used in design calculation. The ratio is also significant in the central and middle side piles in the free-standing group. Generally, for all piles in the free-standing groups and piled raft foundations, the measured bearing capacity is greater than the calculated one, due to the effects of pile installation and stress interaction among adjacent piles and raft. In the free-standing group, only the first factor works. In addition, the stress interactions are little for the single pile in a group and for the corner piles in free-standing group or piled raft. These piles reach their ultimate loads with a settlement of about 20% of their diameters. For the central piles in piled raft and free-standing pile group due to the above-mentioned stress interactions, the corresponding settlement at ultimate load increases. The settlement in the piled raft is also greater than that of free-standing pile due to the raft pressure effect. For the central pile in the 3 × 3 piled raft, the corresponding settlement at ultimate load increases significantly and reaches about 64% of the pile diameter. Corresponding settlement at allowable load is less than 2% of pile diameter for the single pile and about 14% of pile diameter for the central pile in the 3 × 3 piled raft.

In Fig. 19, the load-settlement curve of the piled rafts is compared with that of unpiled raft. By increasing the number of piles, the settlement of the foundation decreases significantly. At the beginning of the loading, due to higher stiffness of the piles than the soil, the slope of load-settlement curves for the piled raft is

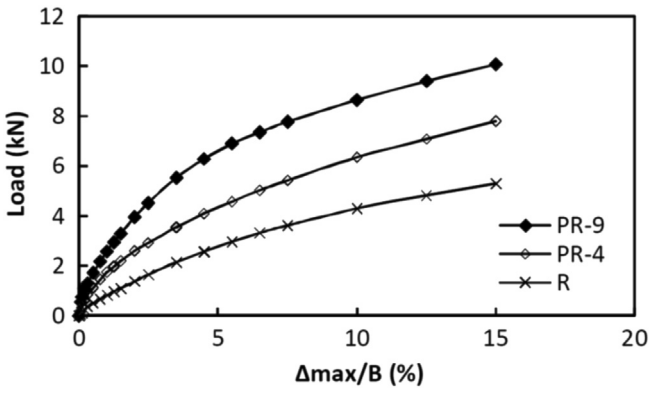

Fig. 19. Average load-settlement relations of unpiled raft, 2 × 2 and 3 × 3 piled rafts.

greater. The piled raft with 9 piles has a steeper initial slope in the loading curve. After pile failure, the loading curve reduces and becomes parallel to that of unpiled raft.

In Fig. 20, the variation of measured total load (pile load plus raft load) with settlement of piled raft is compared to those of free-standing group and unpiled raft. At the initial steps of loading, the curve of the 2 × 2 free-standing group coincides with that of the corresponding piled raft. With elevated pressure beneath the raft, the curves move far away from each other. Because of the low raft pressure in the 3 × 3 piled raft, adjustment of the load-settlement curve of the free-standing group is significant. In Fig. 21, loads of piles within piled raft measured by load cells (without considering the raft load) are determined and compared with that of free-standing group. Since the load cells are not installed on all piles, in this context, it is assumed that the bearing behaviors of the piles in corresponding place are identical. In the 2 × 2 piled raft, due to the minor effect of the raft pressure on corner piles, adjustment of initial part of the curve is marked. In the 3 × 3 piled raft, due to the raft pressure imposed on the central and middle side piles, the pile stiffness will be smaller than those of corresponding piles in the free-standing group. After pile failure due to increasing raft pressure, the pile bearing capacity increases in piled raft and the curves move far away from each other.

The variations of BPI ratio in the test models with the number of piles are shown in Figs. 22 and 23. This ratio decreases with the increasing settlement and reaches a constant value after pile failure (Fig. 24). In the piled raft, the BPI value increases with the increasing number of piles (Fig. 22). In the 2 × 2 free-standing group, BPI reduces to less than one with the increasing settlement to more than about 3% of raft width (Fig. 24).

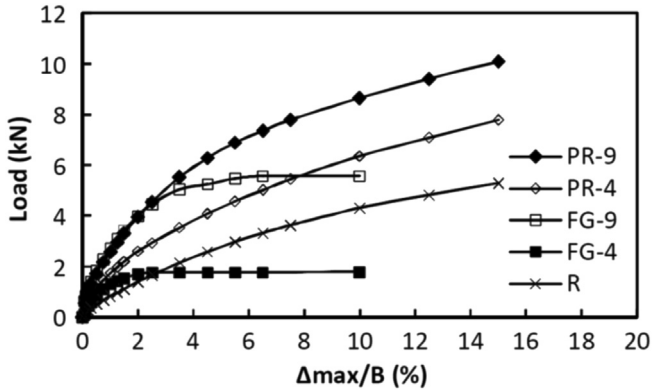

Fig. 20. Average load-settlement relations of unpiled raft, piled raft and free-standing group.

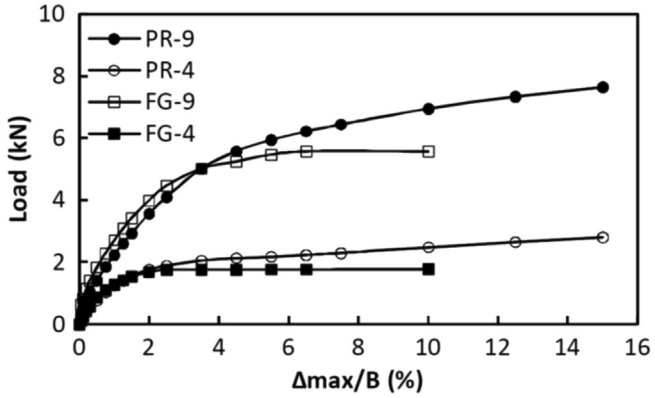

Fig. 21. Variations of pile loads with the ratio of maximum settlement to raft width in piled raft and free-standing group.

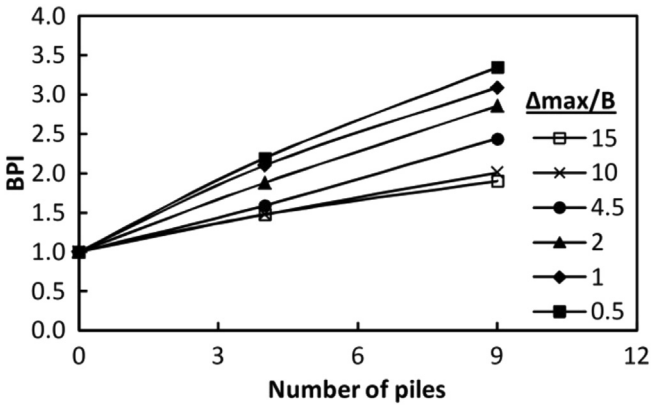

Fig. 22. Variations of bearing improvement ratio (BPI) with the number of piles beneath the raft.

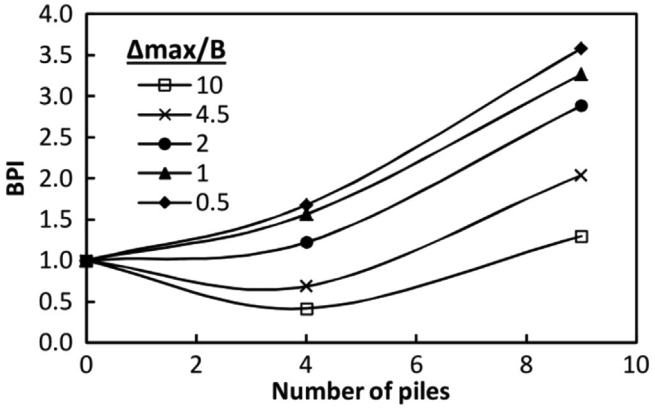

Fig. 23. Variations of BPI with the number of piles in free-standing group.

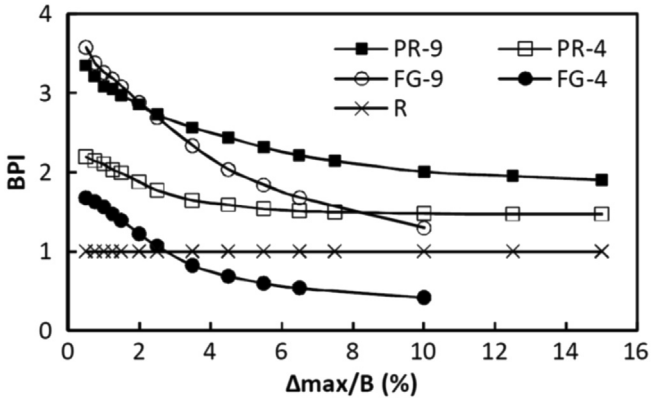

Fig. 24. Variations of BPI with the ratio of maximum settlement to raft width.

The ultimate and allowable loads (Q_u and Q_a) of the models and the corresponding settlement to raft width ratios (S_u/B and S_a/B) are listed in Table 2. By increasing the number of piles beneath the raft, the allowable bearing capacity increases and the corresponding settlement at allowable load reduces.

Fig. 25 illustrates the load-sharing within the piled raft. The pile load-sharing within the piled raft is extrapolated from the load measured by the load cell installed on the planned pile head.

Table 2
Measured allowable and ultimate loads of models and corresponding settlement.

Model	Q_u (kN)	Q_a (kN)	S_u/B (%)	S_a/B (%)
FG-4	1.77	0.59	2.53	0.3
FG-9	5.58	1.86	6.5	0.51
R	4.37	1.46	10	2.09
PR-4	6.37	2.12	10	1.41
PR-9	8.64	2.88	10	1.2

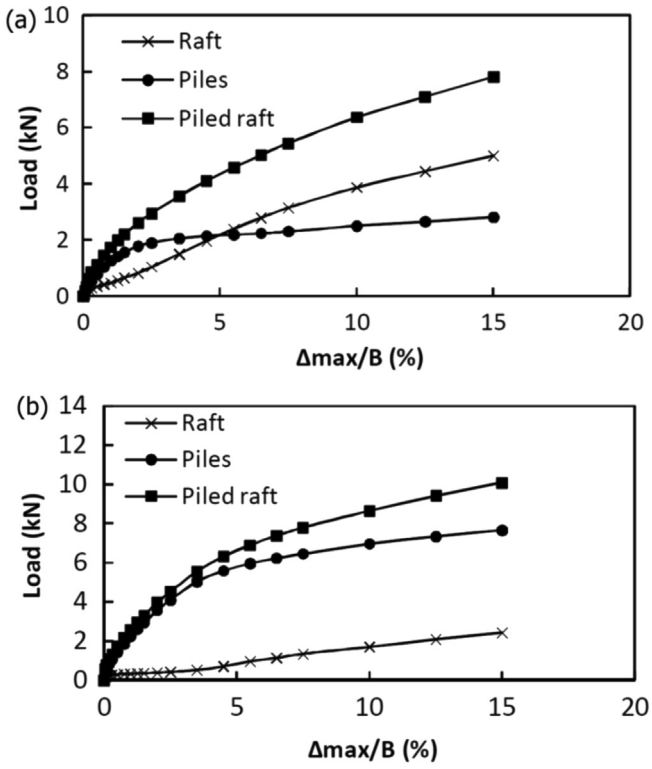

Fig. 25. Load-settlement behaviors of the piles and raft: (a) 2 × 2 piled raft; and (b) 3 × 3 piled raft.

In 2 × 2 piled raft, the pile load is measured in two corner piles and the total load of all piles is extrapolated from multiplication of the average of the two loads by four. In 3 × 3 piled raft, the pile load is measured in corner, middle side and central piles and the total load of all piles is extrapolated from sum of multiplication of corner and middle side pile loads by four and central pile by one. Knowing pile-sharing load, the raft-sharing load is determined by subtracting the pile load from the measured total load. In the 2 × 2 piled raft, at the initial stage of loading, the load-sharing ratio of the piles is larger. After failure of the piles, this distribution will be reversed. In the 3 × 3 piled raft, the piles always tolerate more load than the raft. The load-sharing ratio of each bearing component is shown in Fig. 26. In the 2 × 2 piled raft, the pile load-sharing ratio reaches from 47% to 72%, and to 39% after failure of the piles. In the 3 × 3 piled raft, the pile load-sharing ratio reaches from 67% to 97%, and to 80% at the ultimate load. Therefore, the raft load-sharing ratio varies between 9% and 67% depending on the model properties.

It has been stated that the ultimate load of the piles increases when the piles are installed beneath a raft. On the other hand, by doing this, the raft load is reduced (Fig. 27). These results are also listed in Tables 3 and 4, in which the load-sharing ratios of the piles and raft at the ultimate and allowable loads are illustrated. Since

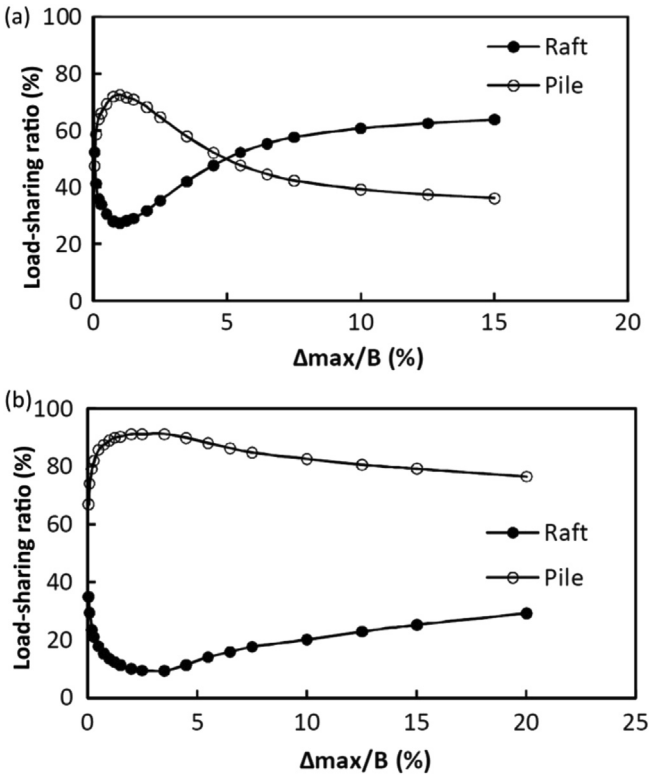

Fig. 26. Load-sharing ratios for raft and piles: (a) 2 × 2 piled raft; and (b) 3 × 3 piled raft.

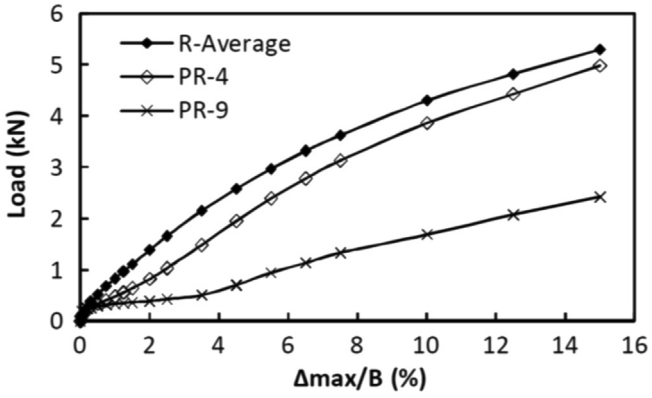

Fig. 27. Bearing behaviors of unpiled and piled rafts.

Table 3
Load-sharing of piles and raft at the ultimate load level.

Model	Q_u (kN)	P (kN)	R (kN)	r_P (%)	r_R (%)	$R/R_{u(ur)}$	$P/P_{us(sum)}$
R	4.31	0	4.31	0	100	1	
PR-4	6.37	2.49	3.87	39.19	60.81	0.9	1.42
PR-9	8.64	6.95	1.69	80.46	19.54	0.39	1.75

Note: P and R are the pile and raft loads, respectively; $R_{u(ur)}$ is the measured ultimate load of the unpiled raft; $P_{us(sum)}$ is the ultimate load of the single piles obtained from multiplying the ultimate load of the single pile by the number of piles; $R_{a(ur)}$ and $P_{as(sum)}$ are the allowable loads obtained from dividing $R_{u(ur)}$ and $P_{us(sum)}$ by the factor of safety of 3, respectively.

the increasing pile load and decreasing raft load mentioned above are not considered in design calculations, the values in the two last columns of Tables 3 and 4 demonstrate the deviations existing in design of piled raft components. As it can be seen, at the allowable

Table 4
Load-sharing of piles and raft at the allowable load level.

Model	Q_a (kN)	P (kN)	R (kN)	r_P (%)	r_R (%)	$R/R_{a(ur)}$	$P/P_{as(sum)}$
R	1.44	0	1.44	0	100	1	
PR-4	2.12	1.51	0.61	71.15	28.85	0.43	2.57
PR-9	2.88	2.53	0.35	87.75	12.25	0.25	1.91

Note: r_P and r_R are the pile and raft load-sharing ratios, respectively.

load level, the amount of the deviation is larger. In the 3 × 3 piled raft, the allowable bearing capacity of the raft is in fact about 25% of the allowable load for the unpiled raft. On the other hand, in this model, the pile bearing capacity is approximately 1.91 times greater than the value considered in the conventional design process.

The amount of the deviation existing in calculating allowable bearing capacity of the piled raft is shown in Table 5. The results are also presented for the free-standing pile group. The allowable bearing capacity of the piles is calculated in two ways, i.e. allowable bearing capacity of the piles without considering the raft bearing capacity, $Q_{a(tra)}$ (conventional approach in the design of piled rafts) and allowable bearing capacity of the piles by considering the raft bearing capacity, $Q_{a(new)}$ (new method). The stress interaction effects on decreasing the raft bearing capacity and increasing the pile bearing capacity are ignored. Based on Table 5, the calculated allowable bearing capacity of the piled raft models by considering the raft load-sharing is in consistent with the measured value. In other words, decreasing the bearing capacity of the raft and increasing the ultimate load of the piles neutralize the effect of each other. Based on the conventional approach without considering the raft load-sharing, the allowable

Table 5
Comparison of measured and calculated bearing capacities of models.

Model	Q_u (kN)	Q_a (kN)	$Q_{a(tra)}$ (kN)	$Q_{a(new)}$ (kN)	$Q_a/Q_{a(tra)}$	$Q_a/Q_{a(new)}$
FG-4	1.77	0.59	0.59	0.59	1.01	1.01
FG-9	5.58	1.86	1.32	1.32	1.41	1.41
R	4.31	1.44	1.44	1.44	1	1
PR-4	6.37	2.12	0.59	2.02	3.62	1.05
PR-9	8.64	2.88	1.32	2.76	2.18	1.04

Table 6
Pile loads at the ultimate and allowable loads of piled raft.

Model	Load type	P_u (kN)	P (kN)	P/P_u (%)
PR-4	Allowable load	0.49	0.38	77.03
PR-9-cor		0.51	0.32	62.63
PR-9-mid		0.72	0.25	34.3
PR-9-cen		1.16	0.26	22.5
PR-4	Ultimate load	0.49	0.62	127.29
PR-9-cor		0.51	0.61	120.52
PR-9-mid		0.72	0.83	114.75
PR-9-cen		1.16	1.19	102.23

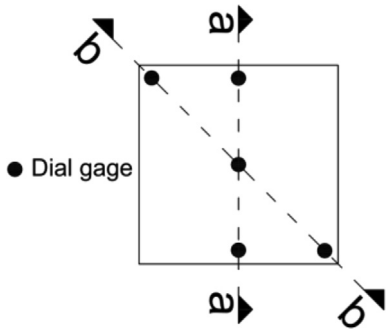

Fig. 28. Arrangements of five dial gages in lateral (a–a) and diagonal (b–b) sections.

bearing capacities are underestimated by greater than 300% and 200% for the 2 × 2 and 3 × 3 piled rafts, respectively. By increasing the pile spacing beneath the raft, the use of the conventional approach becomes more uneconomic.

Table 6 lists the pile loads at the allowable and ultimate loads of the piled raft. At the allowable load of the 2 × 2 piled raft, the pile load exceeds their allowable load and reaches 77% of their ultimate load. In the case of the 3 × 3 piled raft, the corner, middle side and central piles reach 62%, 34% and 22% of the pile ultimate load, respectively. Among these, only the middle side pile provides the factor of safety used in the conventional design calculations. The central pile is far away from its ultimate load. At the ultimate load of the piled raft, all the piles yield and their loads exceed the failure loads, which is due to the raft pressure increase after pile failure. The percentages of the pile load beyond the failure load for the corner, middle side and central piles are 20%, 15% and 2%, respectively. In the central pile due to the increase in stress interaction, the pile failure approximately occurs at the ultimate load of the piled raft.

Table 7 lists the calculated loads of the piles and raft when $Q_{a(tra)}$ and $Q_{a(new)}$ are applied in the piled raft models. The ultimate load of the raft (R_u) considers the measured load of the raft when the maximum settlement equals 10% of the raft width. Therefore, the reduction of the bearing capacity due to the stress interaction is also considered. Based on Table 7, if the raft pressure is ignored and the foundation is designed as a free-standing group, the actual factors of safety for the piles and raft become significantly high. With increasing number of piles and decreasing raft bearing capacity, the factor of safety for the raft decreases. The total factors of safety for the 2 × 2 and 3 × 3 piled rafts are calculated as 10.85 and 6.54, respectively, with the conventional method, verifying that the design method is very uneconomic. By considering the raft pressure, the factors of safety for the piles and raft both decrease. As for the corner piles in the 2 × 2 and 3 × 3 piled rafts, the pile loads exceed their allowable loads, and the factor of safety becomes 1.36 and 1.67, respectively. In contrast, the raft still has a factor of safety greater than 3. These two opposite effects cause the total factors of safety to reach about 3 in

Table 7
Comparison of measured and calculated load capacities of piled raft.

Method	Model	Q_a (kN)	Model	P (kN)	R (kN)	P_u (kN)	R_u (kN)	FS_{Pile}	FS_{Raft}	$FS_{Piled\ raft}$
Conventional method	PR-4	0.59	PR-4	0.09	0.21	0.49	3.87	5.26	18.09	10.85
	PR-9	1.32	PR-9-cor	0.15	0.27	0.51	1.69	3.51	6.31	6.54
			PR-9-mid	0.09		0.72		7.69		
			PR-9-cen	0.1		1.16		12.05		
New method	PR-4	2.02	PR-4	0.36	0.58	0.49	3.87	1.36	6.71	3.15
	PR-9	2.76	PR-9-cor	0.31	0.35	0.51	1.69	1.67	4.86	3.13
			PR-9-mid	0.23		0.72		3.07		
			PR-9-cen	0.25		1.16		4.69		

both models. Therefore, considering the raft load-sharing leads to an economic result.

In Figs. 28 and 29, locations of five dial gages and the distributions of the settlements on the top of the foundation cap in the lateral (a–a) and diagonal (b–b) sections are demonstrated, respectively. Table 8 represents the corner (or middle side) to center deflection ratio (δ/L) and slope of the test models (ζ) in diagonal and lateral sections at the allowable and ultimate load levels, where δ is the differential settlement between the center and corner (in diagonal section) or middle side (in lateral section) of the raft, and L is the distance between the two points. The subscripts 'lat' and 'dia' denote the lateral and diagonal sections, respectively. Generally, the free-standing pile groups at their ultimate and allowable loads tilt less than the corresponding piled

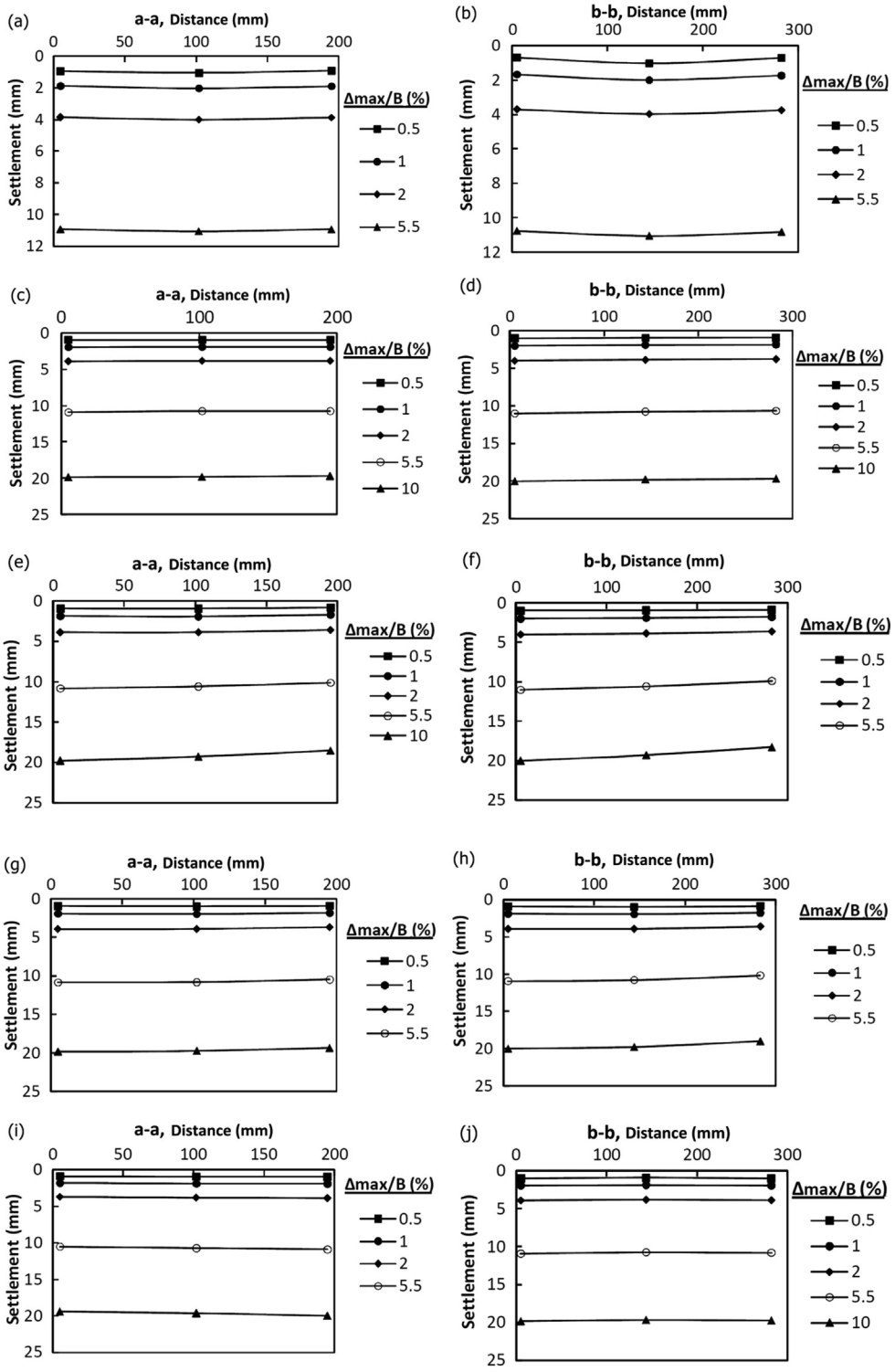

Fig. 29. Raft settlements along sections a–a and b–b: (a, b) FG-4; (c, d) FG-9; (e, f) unpiled raft; (g, h) PR-4; and (i, j) PR-9.

Table 8
The estimated tilts and differential settlements in the models at allowable and ultimate loads.

Model	Load type	Δ_{max}/B (%)	ζ_{lat}	ζ_{dia}	δ/L_{lat}	δ/L_{dia}
FG-4	Allowable	0.3	0.03	0.02	0.04	0.09
FG-9	load	0.51	0.01	0.03	0	0
R		2.09	0.14	0.14	0.05	0.03
PR-4		1.41	0.07	0.08	0.05	0.06
PR-9		1.2	0.03	0.02	0.01	−0.04
FG-4	Ultimate	2.53	0.04	0.04	0.07	0.13
FG-9	load	6.5	0.07	0.12	−0.03	−0.03
R		10	0.65	0.62	0.07	0.08
PR-4		10	0.24	0.35	0.08	0.14
PR-9		10	0.1	0.08	−0.01	−0.08

Table 9
The estimated tilts and differential settlements in the models at allowable load of unpiled raft.

Model	Load (kN)	Δ_{max}/B (%)	ζ_{lat}	ζ_{dia}	δ/L_{lat}	δ/L_{dia}
R	1.44	2.09	0.14	0.14	0.05	0.03
FG-9	1.44	0.31	0.01	0.02	0	0
PR-4	1.44	0.73	0.05	0.02	0.02	0.02
PR-9	1.44	0.36	0.03	0	0.01	−0.04

rafts. The slopes of the raft models at their ultimate loads are greater than those at the allowable loads, but the differential settlements do not change significantly.

In the 2 × 2 piled raft, since the piles are located at the corners, the model becomes bowl-shaped and the differential settlement is greater than those in other models. In the 3 × 3 piled raft, the differential settlement is less than those in other models. Since the external loading area is greater than the central pile area and because of the high bearing capacity of the central pile, the raft becomes dome-shaped. The tilt of the unpiled raft at the allowable load level is greater than those in other models. By increasing the number of piles beneath the raft, the amount of the tilt decreases significantly. Table 9 shows the maximum settlement to raft width ratio (Δ_{max}/B), raft slope (ζ) and the deflection ratio (δ/L) at a constant allowable load of the unpiled raft. Due to the raft pressure in the piled raft models, the foundation stiffness decreases and the deformation of the free-standing pile group becomes less at the same load level. According to Table 9, the unpiled raft shows greater deformation. By increasing the number of piles beneath the raft, the settlement and tilt decrease significantly.

5. Conclusions

A series of loading tests is conducted on single pile, single pile in pile group, unpiled raft, piled raft and free-standing group in sand, and the test results are compared. The precision of available analytical methods in design of piled rafts is investigated. The raft and pile models are made of cast-in-place concrete. Based on the results of the model tests, the following conclusions are drawn:

(1) By installing a single pile in a group, the bearing capacity and stiffness of the pile are increased due to the adjacent pile confinement and increased soil density during pile installation. The increases in bearing capacities of the central, middle side and corner single piles located in the 3 × 3 group ($s/d = 2.6$) are measured to be 57%, 36% and 11%, respectively. This value for the single piles located in the corner of the 2 × 2 group ($s/d = 5.2$) is about 5%. In the piled raft foundation after the pile failure, owing to the increased raft pressure, the stress around the piles is increased and the negative friction occurs, thus the bearing capacity of the piles in the piled raft is greater than that of the free-standing group for the corresponding piles, but the stiffness is lower. The bearing capacity of the central pile in the 3 × 3 piled raft ($s/d = 2.6$) is 2.64 times greater than the single pile capacity. On the other hand, by installation of piles beneath the raft, the bearing capacities of the raft with s/d of 5.2 and 2.6 are reduced by 25% and 43%, respectively. These increases of pile capacity and decrease of raft capacity due to pile interaction and raft pressure have been ignored in available design calculations.

(2) By increasing the number of piles, the settlement of the piled raft decreases significantly. At the initial steps of the loading test, the pile bearing contribution is greater than that of the raft, thus the slope of the load-settlement curve is steeper. After pile failure, the curve is nearly parallel to the load-settlement curve of the unpiled raft.

(3) At the allowable load of piled rafts with s/d of 2.6 and 5.2, the pile load-sharing from the total external load is equal to about 87% and 71%, respectively.

(4) By designing a piled raft based on conventional approach in which the raft load-sharing is not considered, the allowable bearing capacity of the piled raft is underestimated by more than 300% and 200% for s/d of 5.2 and 2.6, respectively. On the other hand, with decreasing number of piles and increasing pile spacing, the conventional method is uneconomic. In contrast, when the raft bearing contribution is considered in the design calculations and the effect of the pile installation on the bearing capacities of the piles and raft is ignored, the difference between the calculated and measured results is insignificant.

(5) At the allowable load level for the piled raft, the pile loads exceed their allowable loads and reach 77% of their ultimate loads for $s/d = 5.2$. In the piled raft with $s/d = 2.6$, the loads of the corner, middle side and central piles reach 62%, 34% and 22% of the ultimate loads of the piles, respectively.

(6) In the 2 × 2 piled raft, due to installation of the piles in the corners of the raft, the raft becomes bowl-shaped after loading, and its differential settlement increases. At the constant allowable load of the unpiled raft, the tilt and settlement are greater than those in other models studied. With increasing the number of piles beneath the raft, the settlement and tilt decrease significantly.

Conflict of interest

We wish to confirm that there are no known conflicts of interest associated with this publication and there has been no significant financial support for this work that could have influenced its outcome.

Notation

B	Raft width
BPI	Bearing pressure improvement ratio
d	Pile diameter
FS_{Pile}	Factor of safety for the pile
FS_{Raft}	Factor of safety for the raft
$FS_{Piled\ raft}$	Factor of safety for the piled raft
L	Corner (middle side) to center distance
P	Pile load
P_a	Measured allowable load of pile
P_u	Measured ultimate load of pile
$P_{a(cal)}$	Calculated allowable load of pile
$P_{us(sum)}$	Summation of equivalent single pile loads
Q_a	Allowable load of test model

Q_u	Ultimate load of test model
$Q_{a(new)}$	Calculated allowable load of piled raft by the new approach
$Q_{a(tra)}$	Calculated allowable load of piled raft by the conventional approach
r_P	Pile load-sharing ratio
r_R	Raft load-sharing ratio
R_u	Measured ultimate load of raft
$R_{u(ur)}$	Measured ultimate load of unpiled raft
S_{Pa}	Settlement of pile at its allowable load
S_{Pu}	Settlement of pile at its ultimate load
S_a	Settlement of test model at its ultimate load
S_u	Settlement of test model at its allowable load
s/d	Pile spacing to diameter ratio
Δ_{max}	Maximum settlement of test model
δ	Differential settlement of test model
δ/L_{lat}	Lateral (middle side to center) deflection ratio
δ/L_{dia}	Diagonal (corner to center) deflection ratio
ζ_{lat}	Lateral slope (tilt) of test models
ζ_{dia}	Diagonal slope (tilt) of test models

References

Alnuaim AM, El Naggar H, El Naggar AM. Evaluation of piled raft performance using a verified 3D nonlinear numerical model. Geotechnical and Geological Engineering 2017;35(4):1831–45.

Altaee A, Fellenius BH. Physical modeling in sand. Canadian Geotechnical Journal 1994;31(3):420–31.

Bazyar MH, Ghorbani A, Katzenbach R. Small-scale model test and three-dimensional analysis of pile-raft foundation on medium-dense sand. International Journal of Civil Engineering 2009;7(3):170–5.

Comodromos EM, Papadopoulou MC, Laloui L. Contribution to the design methodologies of piled raft foundations under combined loadings. Canadian Geotechnical Journal 2016;53(4):559–77.

Dung NT, Chung SG, Kim SR. Settlement of piled foundations using equivalent raft approach. Proceeding of the Institution of Civil Engineers – Geotechnical Engineering 2010;163(2):65–81.

El Sawwaf M. Experimental study of eccentrically loaded raft with connected and unconnected short piles. Journal of Geotechnical and Geoenvironmental Engineering 2010;136(10):1394–402.

El-Garhy B, Galil AA, Youssef A, Raia MA. Behavior of raft on settlement reducing piles: experimental model study. Journal of Rock Mechanics and Geotechnical Engineering 2013;5(5):389–99.

Fioravante V, Giretti D. Contact versus noncontact piled raft foundations. Canadian Geotechnical Journal 2010;47(11):1271–87.

Huang M, Jiu Y, Jiang J, Lie B. Nonlinear analysis of flexible piled raft foundations subjected to vertical loads in layered soils. Soils and Foundations 2017;57(4):632–44.

Lee SH, Chung CK. An experimental study of the interaction of vertically loaded pile groups in sand. Canadian Geotechnical Journal 2005;42(5):1485–93.

Poulos HG, Davis EH. Pile foundation analysis and design. New York: John Wiley and Sons; 1980.

Raut JM, Khadeshwar SR, Bajad SP, Kadu MS. Simplified design method for piled raft foundations. In: Advances in soil dynamics and foundation engineering. American Society of Civil Engineers; 2014. p. 462–71.

Reul O, Randolph MF. Design strategies for piled rafts subjected to nonuniform vertical loading. Journal of Geotechnical and Geoenvironmental Engineering 2004;130(1). https://doi.org/10.1061/(ASCE)1090–0241(2004)130:1(1).

Sedran G, Stolle DFE, Horvath RG. An investigation of scaling and dimensional analysis of axially loaded piles. Canadian Geotechnical Journal 2001;38(3):530–41.

Tagaya K, Scott RF, Aboshi H. Scale effect in anchor pullout test by centrifugal technique. Soils and Foundations 1988;28(3):1–12.

Tomlinson MJ. Pile design and construction practice. 4nd ed. E & FN Spon; 2004.

Mehdi Sharafkhah obtained his BSc degree in University of Science and Technology, Iran and his MSc degree in Babol Noshirvani University of Technology, Iran, in 2008 and 2011, respectively. He is PhD candidate of geotechnical engineering at the Faculty of Civil Engineering, Babol Noshirvani University of Technology, Iran. His research interests include bearing capacity of shallow and deep foundations, foundation settlement, pile design, and experimental studies. He has been participated in a large number of pile and foundation design projects and geotechnical reports in Iran.

Issa Shooshpasha obtained his BSc degree in Tabriz University, Iran in 1987 and his MSc and PhD degrees in McGill University, Montreal, Canada, in 1993 and 1996, respectively. He is associate professor of geotechnical engineering at the Faculty of Civil Engineering, Babol Noshirvani University of Technology, Iran. His research interests include bearing capacity of shallow and deep foundation, slope stability, liquefaction, seepage, soil improvement, and unsaturated soil. He has been participated in a large number of research geotechnical projects in Iran.